COBEM 2021 26th International Congress of Mechanical Engineering
November 22-26, 2021, Virtual Congress, Brazil

COBEM-2021
PARAMETRIC DIFFERENCIAL SENSITIVITY ANALYSIS OF A ONE-DIMENSIONAL THERMAL-ELECTRICAL MODEL OF A PHOTOVOLTAIC SOLAR PANEL

Lucas Haas
Fabiano Cordeiro Cavalcanti
Instituiton: Renewable and Alternative Energy Center (CEAR) in Federal University of Paraíba (UFPB)
Adress: Cidade Universitária - João Pessoa - PB - Brasil - CEP: 58051-970
lucas.haas@cear.ufpb.br, fabianofr@cear.ufpb.br

Cristiane Kelly Ferreira da Silva
Instituiton: Renewable and Alternative Energy Center (CEAR) in Federal University of Paraíba (UFPB)
Adress: Cidade Universitária - João Pessoa - PB - Brasil - CEP: 58051-970
cristianek@cear.ufpb.br

Abstract. *The power and electrical efficiency of a photovoltaic panel decrease with the increase in the temperature of the photovoltaic cell, which makes the determination of this temperature one of the determining factors in the modeling of a photovoltaic panel. In order to precisely determine the temperature of the photovoltaic cell, it is necessary to study the electrical as well as the thermal parameters of the photovoltaic panel, since the temperature of the photovoltaic cell increases with the decrease of the electrical efficiency. The objective of this work is to make a study about the input parameters of a developed thermal-electrical model of a photovoltaic panel, based on a sensitivity analysis. The thermal part of the model is stationary and one-dimensional, where the temperature varies along the five layers of the photovoltaic panel. The electrical part of the model is based on the single diode five parameters model. The coupling of the thermal model with the electrical model was performed through an interactive computational procedure. The input parameters of the thermal-electrical model consist of thermal, electrical, geometric and climatological variables. The parametric study made was based on the differential sensitivity analysis of the temperature of the photovoltaic cell and the electrical efficiency, in relation to the input parameters. The derivatives of the dimensionless sensitivity coefficients were calculated using the central finite difference method. The variations of the sensitivity coefficients along a simulated day were presented in graphs. A discussion about the most important input parameter and its influence on the outputs was made. The inputs that presented the highest averages of the absolute sensitivity coefficients along the day, as an example the air temperature, the transmittance-absorptance product and the open-circuit voltage, are the most important parameters to the estimative of the cell temperature and efficiency. Therefore, these parameters were researched and determined with greater precision, in order to make the model more reliable.*

Keywords: *thermal model, electrical model, sensitivity analysis, photovoltaic cell temperature, photovoltaic panel*

1 INTRODUCTION

According to IEA (2021) electricity generation from photovoltaic (*PV*) solar panels grew 22% in 2019, reaching almost 3% of the total electricity generation in the world. This growing is well on track to reach the Sustainable Development Scenario level by 2030, which will require electricity generation from *PV* panels to increase 15% annually. In order to continue to track this prediction, it is necessary that the research and development of *PV* panels also grow substantially.

Experimental studies on *PV* systems are financially expensive and sometimes unfeasible. Therefore, within a first step, it is recommended that studies be directed from mathematical or computational models, which are able to accurately simulate the behavior of these systems (Jakhrani *et al.*, 2013).

A model of a *PV* panel has the electrical efficiency (η) as one of the main output parameters. The temperature of the photovoltaic cell (T_{cel}) is also important, since η depends on T_{cel} (Skoplaki and Palyvos, 2009). Therefore, to correctly describe the behavior of a *PV* panel, it is necessary to know its thermal parameters as well as the electrical ones. Within this context of inputs of different natures, a more detailed study about those input parameters is indicated.

The objective of this work is to make a study about the input parameters of a developed thermal-electrical model of a *PV* panel. A parametric study that provides good results is the sensitivity analysis (*SA*). *SA* is a method that allows you to classify which inputs cause the most sensitivity in the output. The inputs that have the highest dimensionless sensitivity coefficients are those that need to be thoroughly studied, while the parameters that have the lowest

dimensionless sensitivity coefficients can be studied with less detail (Saltelli *et al*., 2008). Throughout this work, a differential *SA* was made in order to calculate the sensitivity of T_{cel} and η to the different inputs parameters of a developed thermal-electrical model of a *PV* solar panel, in order to determine which inputs are the most important to the calculation of these outputs.

In section 3.1, the input parameters that cause more sensitivity in the outputs T_{cel} and η were presented. A brief discussion was made about how each of the most important inputs exerts its influence on the outputs. In Section 3.2, the general results of the thermal-electrical model applied for the simulation of two days were presented. The results were compared with those of five models found in the literature, three of which are purely thermal models, and two are thermal-electrical models. The made comparison indicated that the calculated T_{cel} is satisfactory, since the calculated T_{cel} is close to the T_{cel} of the other models.

2 MATHEMATICAL MODELLING

The thermal-electrical modeling of the solar *PV* panel is divided into two parts, the thermal and the electrical modeling. This section describes each of these modeling and their coupling into a thermal-electrical model. Before, it is described how the irradiance is calculated using average radiation data obtained from climatological websites such as NASA (2021).

2.1 Climatological Model

The climatological data used in the thermal-electrical model include the monthly average daily total irradiation on a horizontal surface ($\overline{H}$, in kWh/m²/day), the monthly average daily diffuse irradiation on the horizontal surface ($\overline{H}_d$, in kWh/m²/day), the albedo ρ_g (dimensionless), the mean wind speed (V_w, in m/s), and the mean air temperature (T_∞, in ºC). The selected place for the simulation is the Center of Renewable and Alternative Energy (CEAR), located at the Federal University of Paraíba (UFPB), in João Pessoa, Brazil, of latitude ϕ = -7.14º and longitude l = -34.85º. The irradiation $\overline{H}$ is converted into total irradiance on a tilted surface (G_i, in W/m²) in Eq.(1), described in Duffie and Beckmann (2020),

$$G_i = R_b G_b + G_d \left(1 + \frac{\cos\beta_i}{2}\right) + G\rho_g \left(1 - \frac{\cos\beta_i}{2}\right) \quad (1)$$

where R_b (dimensionless) is the ratio of beam irradiance on the tilted surface ($G_{b,T}$, in W/m^2) to that on a horizontal surface (G_b, in W/m^2) at any time; G (in W/m^2) is the total irradiance on a horizontal surface; β_i (in degrees) is the slope angle between the plane of the surface in question and the horizontal plane.

The total irradiance G is calculated with Eq.(2), adapted from Duffie and Beckmann (2020).

$$G = \overline{H}\,\frac{rt}{600}, \quad (2)$$

G_d, in Eq.(1), is also calculated with Eq.(2), replacing $\overline{H}$ for $\overline{H}_d$ and rt for rd. And $G_b = G - G_d$.

2.2 Thermal Model

For the thermal modeling, a steady state and a one-dimensional heat transfer was adopted in the transverse direction to the surface area of the *PV* solar panel. In Figure 1, the temperature of interest to the thermal-electrical model is the temperature of the *PV* cell T_{cel}. To calculate it, an energy balance was carried out that takes into account the energy gains from the irradiance incident on the panel glass G_i, calculated with Eq.(1), and the portion of solar irradiance that is absorbed in the *PV* cells, S (in W/m^2), calculated with Eq.(5). The convective energy losses to the ambient air above and below the panel and the radiative losses from the upper part of the panel to the sky by radiation were also considered in the balance. The radiative losses referring to the lower part of the panel to the neighborhood were neglected. The solar irradiance that is converted into electrical power is represented in Figure 1 by P_{elet}, in W/m². Heat losses are represented by the resistances to convection $R''_{conv,sup}$ and $R''_{conv,inf}$, and the resistance to radiation R''_{rad}, in m²K/W (Incropera *et al*., 2017), in Figure 1. The subscripts *sup* and *inf* refer to the upper and lower surfaces of the *PV* panel. The resistances $R''_{mod,sup}$ and $R''_{mod,inf}$, also in m²K/W, represent the equivalent resistances to the heat conduction between the different layers of the panel, specified to the left of the thermal circuit in Figure 1. T_g, T_∞ and T_{sky} are the temperatures of the upper surface of the glass, of the ambient air and of the sky, in °C. A thermal balance was carried out on the two unknowns, T_{cel} and T_g.

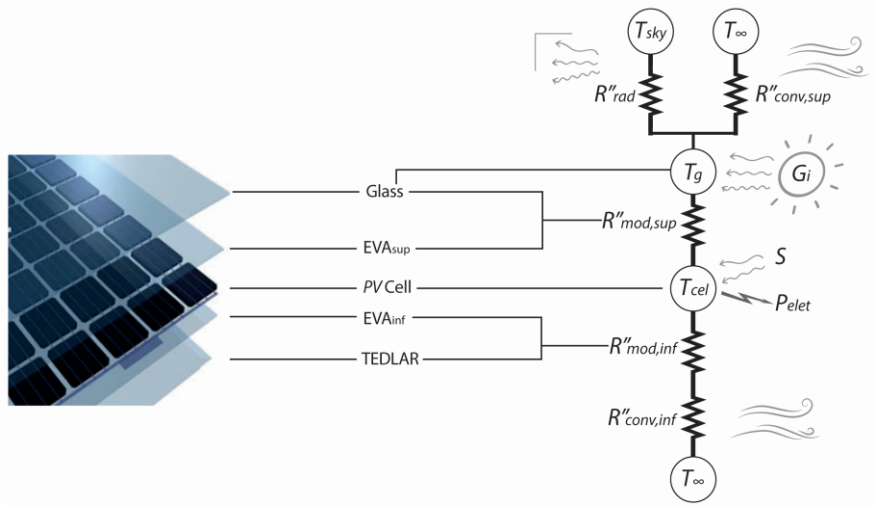

Figure 1. *PV* solar panel layers and the thermal equivalent circuit.

Thermal balance on T_g:

$$\frac{T_\infty - T_g}{R''_{conv,sup}} + \frac{T_{sky} - T_g}{R''_{rad}} + \alpha_g G_i + \frac{T_{cel} - T_g}{R''_{mod,sup}} = 0 \tag{3}$$

The parameter α_g (dimensionless) in Eq.(3) is the glass absorptance of solar radiation. T_{sky} was obtained using the aproximation described in Duffie and Beckmann (2020), where $T_{sky} = T_\infty - 5$.

Thermal balance on T_{cel}:

$$\frac{T_g - T_{cel}}{R''_{mod,sup}} + \frac{T_\infty - T_{cel}}{R''_{conv,inf} + R''_{mod,inf}} + S = \eta G_i \tag{4}$$

In Eq.(4), η (dimensionless) is the electrical efficiency, calculated with the electrical model. S (in W/m^2) is the irradiance that is absorbed on the *PV* cell. S is calculated with the Eq.(5) (Notton *et al.*, 2005),

$$S = \alpha_{cel}\tau_g \left(R_b K_b G_b + G_d K_d \left(1 + \frac{cos\beta_i}{2}\right) + G\rho_g K_g \left(1 - \frac{cos\beta_i}{2}\right)\right) \tag{5}$$

where $\alpha_{cel}\tau_g$ (dimensionless) is the product of the transmittance of the glass with the absorptance of the *PV* cell for the normal incident solar irradiance. The dimensionless parameters K_b, K_d and K_g in Eq.(5) are the incident angle modifiers of the beam, diffuse and ground-reflected solar irradiance, respectively (Notton *et al.*, 2005).

2.3 Electrical Model

The electrical model was developed from the electrical circuit that represents a *PV* solar panel in Figure 2. The *PV* panel circuit has a current source that represents the photogenerated current (I_{pv}, in A), a diode that consumes an amount of current (I_d, in A) which includes the reverse saturation current (I_0, in A), and two resistances that represent the losses of the *PV* panel. The parallel resistance (R_p, in Ω) represents the losses due to leakage current, which depends on the manufacturing method used, and the series resistance (R_s, in Ω) represents the structural losses of the *PV* panel, such as the losses from cable connections and electrical welding (VILLALVA *et al.*, 2009).

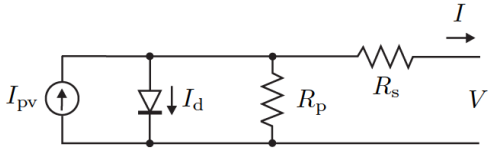

Figure 2. Single-diode and two resistances equivalent electrical circuit of a *PV* panel.

Equation (6) represents the electrical circuit in Figure 2 (Villalva *et al.*, 2009).

$$I = I_{pv} - I_o\left[\exp\left(\frac{V+R_S I}{V_t\, a}\right) - 1\right] - \frac{V+R_S I}{R_p} \tag{6}$$

The developed electrical model is based on the model by Villalva *et al.* (2009). To find out the voltage (*V,* in V*)* and current (*I,* in A) generated by the *PV* solar panel, it is necessary to first calculate the five unknown parameters in Eq.(6): I_{pv}, R_p, R_s, a and I_0. The three parameters reverse saturation current (I_0), photogenerated current (I_{pv}) and diode ideality constant (a) are functions of the other two unknown parameters, R_p and R_s. The parameters R_p and R_s need an iterative process to be calculated, in which R_p is calculated for the R_s values $0 < R_s < R_{s,max}$, until a pair of R_p and R_s that makes $P_{calc} = P_{stc}$ is found, where P_{stc} (in W) is the standard power provided by the manufacturer and $P_{calc} = V.I$ (Villalva *et al.*, 2009). Finally, the efficiency η is calculated with Eq.(7),

$$\eta = \frac{P_{calc}}{G_i.area}, \tag{7}$$

where *area* is the *PV* solar panel area, in m².

After calculating R_p and R_s for the Standard Test Conditions *STC* (G_i = 1000W/m², T_{cel} = 25°C) it is possible to calculate η for other climatic conditions beside the *STC* conditions using the same R_p and R_s. The parameter V in Eq.(6) could be any value between $0<V<V_{oc}$, where V_{oc} (in V) is the open–circuit voltage. A control method is needed to find the pair of V and I that calculates the highest power (P_{calc}). An easy way to find the highest P_{calc} in a computational model is to calculate all P_{calc} for the $0<V<V_{oc}$ values, and to search for the highest P_{calc}.

2.4 Coupling of the Thermal and Electrical Models

The first step to calculate the coupled solution of the thermal-electrical model consists of solving the electrical part of the model, in order to calculate an initial value for η. For this first solution of η, an initial temperature is assigned to the *PV* cell, $T_{cel,initial}$. Then, the thermal part of the thermal-electrical model is solved, which calculates a T_{cel} based on the η previously calculated. Then, the two temperatures, T_{cel} and $T_{cel,initial}$, are compared. If the absolute difference between T_{cel} and $T_{cel,initial}$ is greater than or equal to the error, $T_{cel,initial}$ becomes equal to T_{cel}. The electrical model is then restarted. If the new difference is smaller than the error, the program ends with the final value for T_{cel}. The basic scheme of the described procedure is shown in Figure 3. The program runs for each of the 78 10-minutes intervals between sunrise and sunset, for each simulated day.

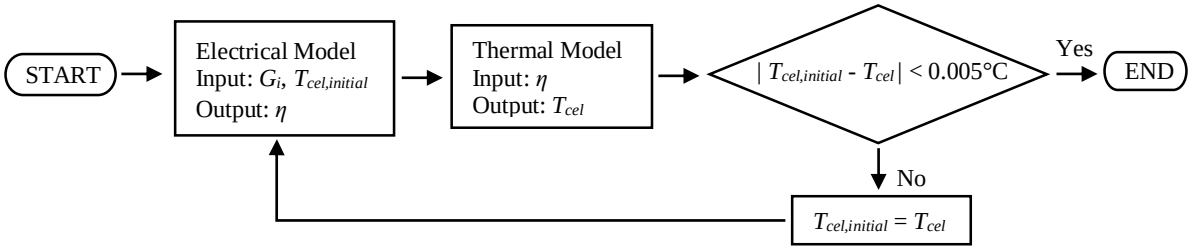

Figure 3. Algorithm of the coupling of the thermal and electrical models.

2.5 Sensitivity Analysis

The parametric study that was made about the thermal-electrical model was based on the differential sensitivity analysis (*SA*) described in Saltelli *et al.* (2008). *SA* is a useful tool that helps to make decisions about a model. The *SA* results serve as justification for using or not a consideration. The *SA* was made for the average day of November (November 14). November is the month that presents the highest value of monthly average daily total radiation $\bar{H}$ for the selected location (NASA, 2021).

The operating scheme of the program developed in MATLAB to perform the *SA* is shown in Figure 4. First, the thermal-electrical model program runs with the standard inputs, in order to calculate the standard outputs η_0 and $T_{cel,0}$. The selected input from which the sensitivity analysis will be performed becomes x_0. x_0 is incremented for more (x_p) and for less (x_n). The thermal-electrical program is executed twice more, once with the input x_p in order to calculate the outputs η_p and $T_{cel,p}$, and once again with the input x_n in order to calculate the outputs η_n and $T_{cel,n}$. The partial derivatives $\partial\eta/\partial x$ and $\partial T_{cel}/\partial x$ are calculated using the centered finite difference method, described in Li *et al.* (2018).

Afterwards, the partial derivatives are multiplied by the input at his standard value (x_0), and divided by the standard output value (η_0 or $T_{cel,0}$), thus arriving at the dimensionless sensitivity coefficient of T_{cel} in relation to input x ($J_{Tcel,x}$),

and the dimensionless sensitivity coefficient of η in relation to x ($J_{\eta,x}$). The program comes to an end, and another input parameter can be selected to restart the program.

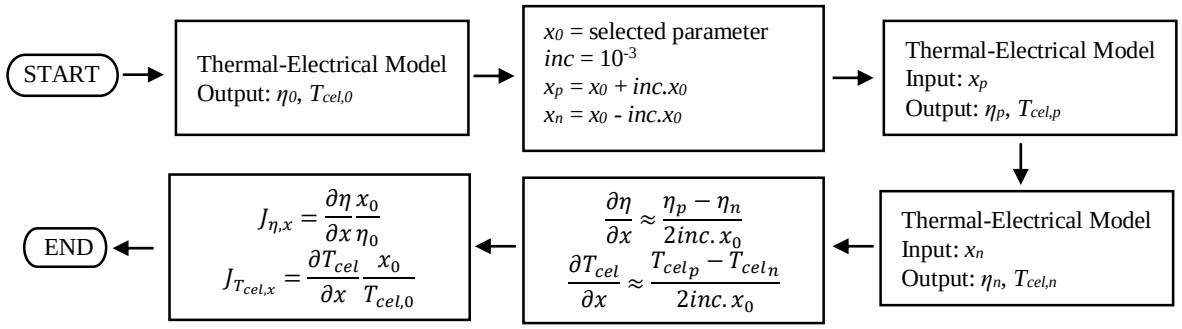

Figure 4. Algorithm of the sensitivity analysis model.

The most important input parameters to the T_{cel} and η outputs, used in the thermal modeling described in Section 2.2 and in the electrical modeling described in Section 2.3, are shown in Table 1.

Table 1. Most important inputs of the thermal-electrical model

INITIALS	DESCRIPTION	VALUE
α_g	Glass absorptance	0.05 ± 0.0025
ε_g	Glass emissivity	0.91 ± 0.0455
$\tau_g\alpha_{cel}$	Transmittance-absorptance product	0.855 ± 0.0428
β_i	Slope	10 ± 0.1 °
L	*PV* panel length	1.956 ± 0.0005 m
$area$	*PV* panel area	1.940 ± 0.011 m²
$\bar{H}$	Monthly average daily total radiation	21.924 ± 2.192 MJ/m².dia (1)
T_∞	Mean air temperature	26.61 ± 0.2 °C (1)
V_w	Mean wind speed	4.45 ± 0.0445 m/s (1)
a	Diode ideality constant	1.07 ± 0.0535
I_{scn}	Standard short-circuit current	9.22 ± 0.338 A
V_{ocn}	Standard open-circuit voltage	47 ± 0.545 V
K	Air thermal conductivity	26.7 ± 1.335 mW/m.K (2)
Pr	Prandtl number	0.706 ± 0.0353 (2)
v	Air kinematic viscosity	16.5 ± 0.825 .10^{-6} m²/s (2)

(1) varies according to the day. The presented value is for November 14.
(2) varies along the day. The presented value is the average value for November 14.

3 RESULTS AND DISCUSSION

The sensitivity of T_{cel} and η to the most important input parameters are shown and a discussion about each of these inputs is made. Then, the calculated T_{cel} and η are compared with five other models.

3.1 Differencial Sensitivity Analysis

The *SA* program (Figure 4) was run for each of the 78 intervals of the day for all inputs. Thus, the variations throughout the day of the dimensionless sensitivity coefficients $J_{Tcel,x}$ and $J_{\eta,x}$ were calculated. Table 2(a) presents the data regarding the most important dimensionless sensitivity coefficients of the *PV* cell temperature in relation to the x inputs ($J_{T_{cel},x}$). The third column of the Table presents $MEAN(|J_{T_{cel},x}|)$, which represents the average of the absolute values of each $J_{T_{cel},x}$ throughout the day. The coefficients $J_{T_{cel},x}$ were sorted in descending order of $MEAN(|J_{T_{cel},x}|)$. Table 2(b) presents the same type of data, but referred to the sensitivity of η: $J_{\eta,x}$ and $MEAN(|J_{\eta,x}|)$.

Table 2. Ranking of the most important inputs to the outputs a) T_{cel} and b) η.

(a)

RANKING	x	$MEAN(\lvert J_{T_{cel},x} \rvert)$
1º	T_∞	0.85226
2º	$\tau_g\alpha_{cel}$	0.05363
3º	$\bar{H}$	0.04228
4º	K	0.02421
5º	ε_g	0.01600
6º	V_w	0.01596
7º	L	0.01593
8º	v	0.01210
9º	V_{ocn}	0.00831

(b)

RANKING	x	$MEAN(\lvert J_{\eta,x} \rvert)$
1º	V_{ocn}	1.20930
2º	T_∞	1.12450
3º	$\bar{H}$	0.97311
4º	$area$	0.86720
5º	I_{scn}	0.81511
6º	a	0.23336
7º	β_i	0.08653
8º	$\tau_g\alpha_{cel}$	0.07534
9º	β	0.07301

Figure 5 shows the variation of the dimensionless sensitivity coefficients $J_{T_{cel},x}$ throughout the simulated day. The farther the $J_{T_{cel},x}$ is from the axis where $J_{T_{cel},x}$= 0, the more sensitive is the output T_{cel} with respect to input x. The order of presentation of the x inputs in the legend of Figure 5(a) and Figure 5(b) is the same order as the ranking of the Table 2(a).

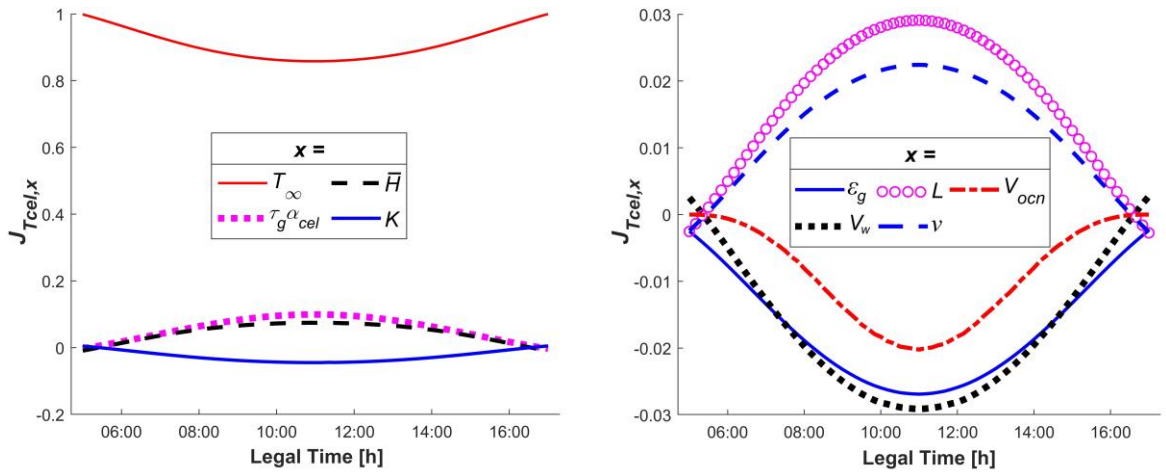

Figure 5. Sensitivity coefficients of T_{cel} ($J_{T_{cel},x}$) to the variations of the x inputs.

It can be observed in Figure 5 that the dimensionless sensitivity coefficients $J_{T_{cel},x}$ are always more distant from the axis where $J_{T_{cel},x}$= 0 at solar noon, that is, the $J_{T_{cel},x}$ are more significant at this time, with the only exception being the dimensionless sensitivity coefficient of T_{cel} to the input air temperature (J_{T_{cel},T_∞}), which is more significant at the beginning and end of the day. The increase in the significance of the others $J_{T_{cel},x}$ when close to solar noon occurs because at this time the absolute value of the derivatives $\partial T_{cel}/\partial x$ are greater. And the derivatives $\partial T_{cel}/\partial x$ are greater when close to solar noon due to the increase of G_i and S at this time, according to Eq.(1) and Eq.(5).

The parameter T_∞, in Figure 5(a), is the input that most influences the determination of T_{cel}, because its sensitivity coefficient (J_{T_{cel},T_∞}) is the highest. A positive increment in T_∞ causes a positive increment in T_{cel}. In practice, this is because the heat transfer by convection is proportional to the temperature difference between the external surfaces of the PV panel and T_∞. In the developed model, T_∞ is used to calculate the sky temperature (T_{sky}), used in Eq.(3), and the temperature at which the air parameters conductivity (K), Prandtl number (Pr) and kinematic viscosity (v) are calculated. K, Pr and ν are used to calculated the convective resistances $R''_{conv,sup}$ and $R''_{conv,inf}$, in Eq.(3) and Eq.(4).

The second highest sensitivity coefficient of T_{cel} is the sensitivity to the variable $\tau_g\alpha_{cel}$ ($J_{T_{cel},\tau_g\alpha_{cel}}$), in Figure 5(a). The variable $\tau_g\alpha_{cel}$ represents the fraction of the solar irradiance G_i that is transmitted by the glass and absorbed on the PV cell. An increase in $\tau_g\alpha_{cel}$ causes an increase in the portion of irradiance that is absorbed in the cell (S), according to

the Eq.(5), causing a greater portion of the irradiance to be converted into heat in the *PV* cell, increasing T_{cel}. A positive increment in $\tau_g \alpha_{cel}$ causes a positive increment in T_{cel}.

The sensitivity coefficient $J_{T_{cel},\bar{H}}$ in Figure 5(a) shows how much sensitive T_{cel} is to the variation of the total horizontal solar irradiation $\bar{H}$. The parameter $\bar{H}$ is used in the Eq.(2), so that the incident irradiance (G_i) and the irradiance absorbed in the *PV* cell (S) can be calculated, respectively, with Eq.(1) and Eq.(5). A positive increment in $\bar{H}$ causes a positive increment in T_{cel}.

The sensitivity coefficient $J_{T_{cel},K}$ in Figure 5(a) shows how much sensitive T_{cel} is to the variation of the thermal conductivity of the air K. The parameter K is used to calculate the convective resistances $R_{conv,sup}$ e $R_{conv,inf}$ used in the thermal balance of Eq.(3) and Eq.(4). The larger the K, the more convective transfer the *PV* panel performs with the ambient air. Therefore, a positive increment in K causes a negative increment in T_{cel}, making $J_{T_{cel},K}$ negative.

The sensitivity coefficient $J_{T_{cel},\varepsilon_g}$ in Figure 5(b) shows how much sensitive T_{cel} is to the variation of the emissivity of the glass ε_g. The parameter ε_g is used to calculate the radiation resistance in Eq.(3). The larger the ε_g, the more energy the glass loses to the sky by long wavelength radiation, causing the *PV* panel temperatures, which include T_{cel}, to decrease. Therefore, a positive increment in ε_g causes a negative increment in T_{cel}, making $J_{T_{cel},\varepsilon_g}$ negative.

The sensitivity coefficient J_{T_{cel},V_w} in Figure 5(b) shows how much sensitive T_{cel} is to the variation of the wind speed V_w. The parameter V_w is used to calculate the convective resistances used in the thermal balances in the Eq.(3) and Eq.(4). The larger the V_w, the more energy the *PV* panel loses by convection. A positive increment in V_w causes a negative increment in T_{cel}, making J_{T_{cel},V_w} negative.

The sensitivity coefficient $J_{T_{cel},L}$ in Figure 5(b) shows how much sensitive T_{cel} is to the variation of the length of the *PV* panel L. The parameter L is used to calculate the convective resistances $R''_{conv,sup}$ and $R''_{conv,inf}$ used in the thermal balances in the Eq.(3) and Eq.(4). The larger the L, the larger is the convective resistances, and less energy the *PV* panel loses by convection. A positive increment in L causes a positive increment in T_{cel}.

The sensitivity coefficient $J_{T_{cel},\nu}$ in Figure 5(b) shows how much sensitive T_{cel} is to the variation of the air kinematic viscosity ν. The parameter ν is used to calculate the convective resistances used in the thermal balances in the Eq.(3) and Eq.(4). The larger the ν, less energy the *PV* panel loses by convection. A positive increment in ν causes a positive increment in T_{cel}.

The sensitivity coefficient $J_{T_{cel},V_{ocn}}$ in Figure 5(b) shows how much sensitive T_{cel} is to the variation of the standard open-circuit voltage V_{ocn}. In practice, an increase in V_{ocn} causes an increase in the maximum power voltage V_{mp}, which causes an increase in the electrical efficiency η. The increase in η causes a smaller portion of the irradiance absorbed in the *PV* cell to be converted into thermal energy, causing T_{cel} to decrease. In the modeling, V_{ocn} is used to calculate the reverse saturation current I_0, used in the Eq.(6). The larger the V_{ocn}, the smaller is I_0, and less G_i is converted into thermal energy. A positive increment in V_{ocn} causes a negative increment in T_{cel}, making $J_{T_{cel},V_{ocn}}$ negative.

The variations of the most important sensitivity coefficients of the output η ($J_{\eta,x}$) are shown in Figure 6.

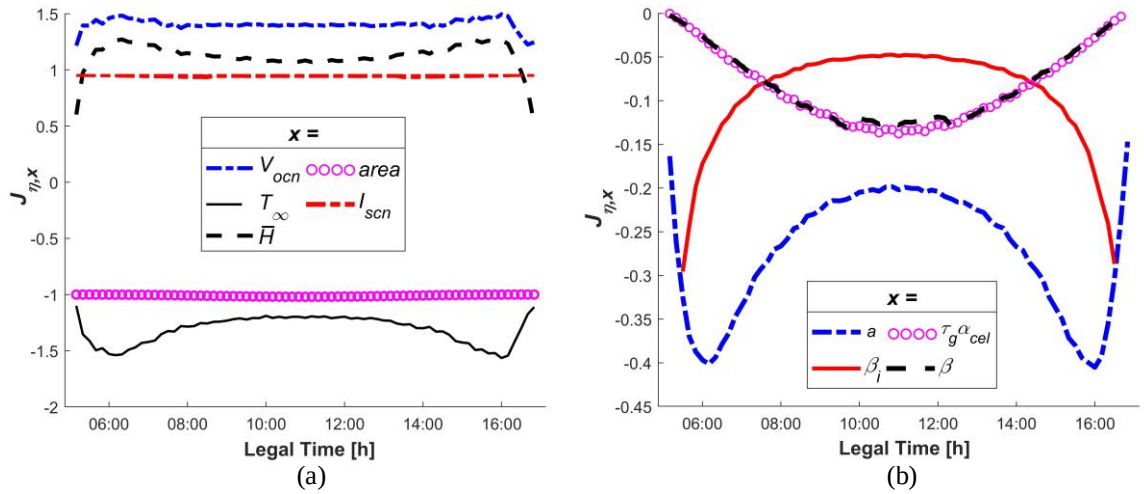

Figure 6. Sensitivity coefficients of η ($J_{\eta,x}$) to the variations of the x inputs.

The parameter V_{ocn}, in Figure 6(a), is the input that most influences the determination of η, because its sensitivity coefficient ($J_{\eta,V_{ocn}}$) is the highest. In practice, an increase in V_{ocn} causes an increase in the maximum power voltage V_{mp}, which causes an increase in η. In the modeling, V_{ocn} is used to calculate the leakage current I_0, used in Eq.(6). The larger the V_{ocn}, the smaller is I_0, causing an increase in η. A positive increment in V_{ocn} causes a positive increment in η.

The second highest sensitivity coefficient of η is the sensitivity to the variable T_∞ (J_{η,T_∞}), in Figure 6(a). An increase in T_∞ causes an increase in T_{cel}, which causes a decrease in η. A positive increment in T_∞ causes a negative increment in η, making J_{T_{cel},T_∞} negative.

The sensitivity coefficient $J_{\eta,\bar{H}}$ in Figure 6(a) shows how much η is sensitive to the variation of the total horizontal solar irradiation $\bar{H}$. $\bar{H}$ is used in Eq.(2), so that the incident irradiance G_i can be calculated with Eq.(1). The photogenerated current I_{pv}, used in Eq.(6), increases with the growth of G_i, causing an increase in η. A positive increment in $\bar{H}$ causes a positive increment in η.

The sensitivity coefficient $J_{\eta,area}$ in Figure 6(a) shows how much η is sensitive to the variation of the area of the *PV* panel. The parameter *area* is used in Eq.(7) to calculate η. A positive increment in *area* causes a negative increment in η, making $J_{\eta,area}$ negative.

The sensitivity coefficient $J_{\eta,I_{scn}}$ in Figure 6(a) shows how much sensitive η is to the variation of the standard short-circuit current I_{scn}. In practice, an increase in I_{scn} causes an increase in the maximum power current I_{mp}, which causes an increase in η. In the modeling, I_{scn} is used to calculate the photogenerated current I_{pv}, used in Eq.(6). The larger the I_{pv}, the larger is η. A positive increment in I_{scn} causes a positive increment in η.

The sensitivity coefficient $J_{\eta,a}$ in Figure 6(b) shows how much η is sensitive to the variation of the diode ideality constant a. The larger the parameter a, less idealized the diode is, and less current the panel generates for a given voltage. A positive increment in a causes a negative increment in η, making $J_{\eta,a}$ negative.

The sensitivity coefficient J_{η,β_i} in Figure 6(b) shows how much η is sensitive to the variation of the slope of the *PV* panel β_i. The simulated *PV* panel has a slope of β_i = 10° from the horizontal, with the collector facing the geographical north. The latitude of the simulation site is ϕ = -7.14°, while the solar declination on the day selected for the analysis (November 14) is δ = -19°. That is, while the *PV* panel is tilted to the north, the Sun makes its apparent trajectory to the south of the simulation site. By increasing β_i, the solar irradiance becomes even less perpendicularly on the *PV* panel, causing a decrease in G_i and η. A positive increment in β_i causes a negative increment in η, making J_{η,β_i} negative.

The sensitivity coefficient $J_{\eta,\tau_g\alpha_{cel}}$ in Figure 6(b) shows how much η is sensitive to the variation of the product of the short waves transmittance of the glass with the absorptance of the *PV* cell, $\tau_g\alpha_{cel}$. The parameter $\tau_g\alpha_{cel}$ is used to calculate the amount of irradiance that is absorbed by the cells (S) in Eq.(5). The increase in S, which is caused by the increase in $\tau_v\alpha_{cel}$, causes an increase in T_{cel}, which causes a decrease in η. A positive increment in $\tau_v\alpha_{cel}$ causes a negative increment in η, making $J_{\eta,\tau_g\alpha_{cel}}$ negative.

The sensitivity coefficient $J_{\eta,\beta}$ in Figure 6(b) shows how much sensitive η is to the variation of the thermal coefficient of the standard open-circuit voltage β. The parameter V_{ocn} is used to calculate the generated voltage V. The greater the β, the less V is generated for a given temperature and the lower is the efficiency η. A positive increment in β causes a negative increment in η, making $J_{\eta,\beta}$ negative.

3.2 Results of the Thermal-Electrical Model

The results of the Sensitivity Analysis established which inputs parametrs are the most important to the developed thermal-electrical model, so that the uncertainties of these parameters could be determined with more precision than the uncertainties of the less important parameters. With the most important uncertainties established (Table 1), it is possible to determine the total uncertainty of the model outputs T_{cel} and η. Figure 7 and Figure 8 presents the results of the thermal-electrical model for the average days that represent the summer and winter solstices months, June 11 (T_∞ = 25,61 °C, V_w = 4,44m/s, $G_{i,max}$ = 640,35 W/m²) and December 10 (T_∞ = 27,07 °C, V_w = 4,30 m/s, $G_{i,max}$ = 796,72 W/m²), where $G_{i,max}$ is the maximum irradiance, found at solar noon.

The results of T_{cel} and η of the developed thermal-electrical model, presented as *TE Haas* in Figure 7 and Figure 8, were plotted as a function of the standard time of day - from sunrise to sunset, in 78 intervals of 10 minutes. The results were compared with the results of five other models found in the literature, three of them being the purely thermal models *T NOCT* (Ross, 1976), *T Risser* (Risser and Fuentes, 1984) and *T Ross* (Ross, 1986), and the two thermal-electrical models *TE King* (King *et al*., 2004) and *TE Smets* (Smets *et al*., 2016).

It can be seen in Figure 7(a) and Figure 8(a) that the minimum T_{cel} ($T_{cel,min}$) is always found at the beginning and end of the day for all models. The purely thermal models *T NOCT* and *T Ross* and the thermal-electrical model *TE King* have $T_{cel,min} = T_\infty$, while the *T Risser* model has $T_{cel,min} > T_\infty$. The *TE Haas* and *TE Smets* models have $T_{cel,min} < T_\infty$, because at this time they lose thermal energy via radiation to the sky. The T_{cel} values of the *T NOCT* and *T Ross* models are within the uncertainty bars of the *TE Haas* model for most of the day, while the T_{cel} values of the *T Risser* model is almost half of the day within the *TE Haas* uncertainty bars.

Pure thermal models make a good estimate of the *PV* cell temperature. However, the effect of the T_{cel} variation alone is not enough to correctly predict the variation in the efficiency throughout the day, in Figure 7(b) and Figure 8 (b). The efficiency of the purely thermal models *T NOCT*, *T Risser* and *T Ross* only take into account the influence of T_{cel} in η, disregarding the influence of G_i in η. The η of these models present their highest values at the beginning and at the end of the day, when $T_{cel,min}$ is found. However, at these times, when there is no solar radiation, the current I_{pv} is

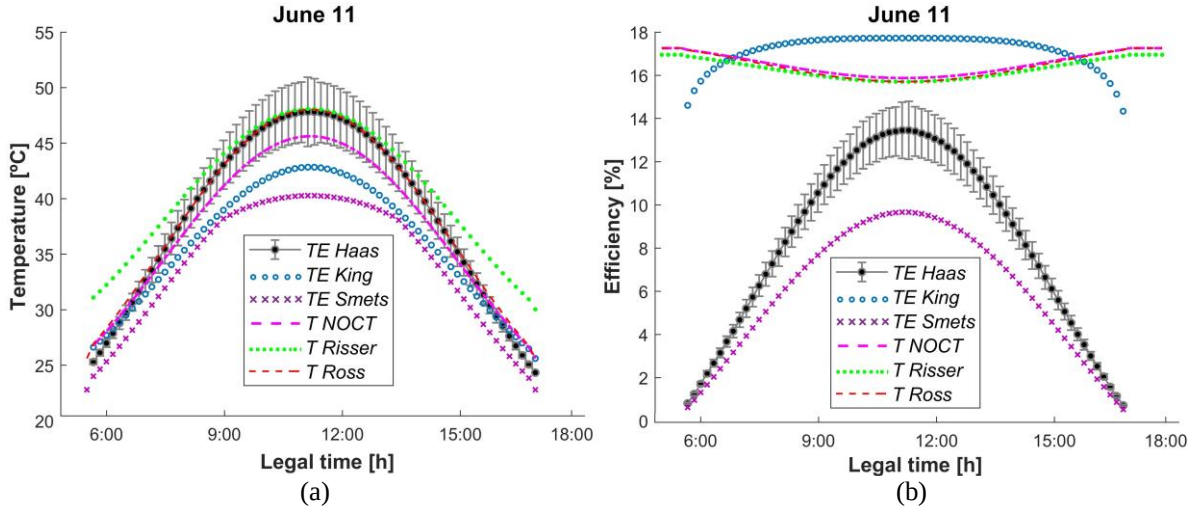

Figure 8 - Results of the thermal-electrical model (*TE Haas*) for June 11, compared with five other models, for a) T_{cel} and for b) η.

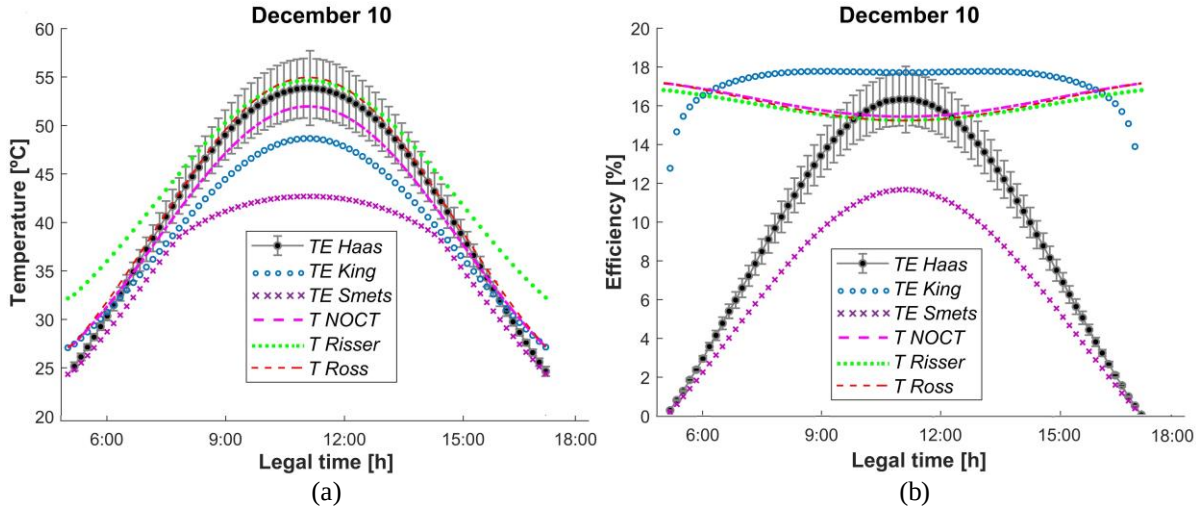

Figure 7 - Results of the thermal-electrical model (*TE Haas*) for December 10, compared with five other models, for a) T_{cel} and for b) η.

equal to 0, which makes η equal to 0 as well. (DURISCH *et al.*, 2007). Thus, it is expected that the models that start the day with $\eta = 0$, like the *TE Haas* and *TE Smets* models, tend to better describe the behavior of η throughout the day. The *TE Haas* and *TE Smets* models take more into account the influence of G_i on η than the influence of T_{cel} on η, causing the largest η to be found at solar noon. The efficiency of the *TE King* model is higher than the efficiency given by the manufacturer $\eta_{stc} = 17.3\%$ at some times of the day, indicating that this model overestimates the efficiency. None of the efficiencies of the five models compared are within the error margins of the η of the developed model for a considerable time.

4 CONCLUSION

Photogenerated energy varies according to the climatic conditions of the installation site, and the study of this variation deserves attention. A *PV* solar panel depends not only on the electrical parameters, but also on the thermal ones. In this work, a mathematical model of a *PV* panel was developed in order to obtain more realistic data regarding the generated energy. A parametric study based on a sensitivity analysis was made regarding the thermal-electrical model inputs.

The dimensionless sensitivity coefficients of the outputs T_{cel} and η regarding the input parameters were calculated. Their variations along the day were presented in graphs. A ranking of the most important input parameters was created using the averages of the absolute values of the dimensionless sensitivity coefficients along the day. The sensitivity coefficients regarding the climatic parameters T_∞ and $\overline{H}$ are two of the three highest sensitivity coefficients as much for

T_{cel} as for η, indicating that these climatic parameters are the most important inputs to the developed thermal-electrical model. Other important inputs are V_{ocn}, which has the highest sensitivity coefficient of η, and $\tau_g\alpha_{cel}$, which has the third highest sensitivity coefficient of T_{cel}. Of these mentioned input parameters, the input with the fewest references in the literature is $\tau_g\alpha_{cel}$, indicating that, to develop an accurate thermal-electrical model of a *PV* panel, the transmittance of the glass and the absorptance of the cell are the parameters that need the most to be researched.

The sensitivity analysis was made for one day. Due to the non-linearity of the model, the *SA* results are applicable only for the day on which the *SA* was performed, so care must be taken if applying the results for other days. The parametric study that was made generated more knowledge about the functioning of the model, making it more reliable. From the *SA* it was also possible to estimate the uncertainty ranges for T_{cel} and η. The results for T_{cel} and η were presented and compared with the results from five other models. Some of these models presented a T_{cel} within the error bars of the T_{cel} calculated by the developed model, indicating that the developed model makes a good estimate of T_{cel}.

1. REFERENCES

Duffie, J. A., Beckman, W. A, Blair N., 2020. *Solar Engineering of Thermal Processes, Photovoltaics and Wind*. John Wiley & Sons.

Durisch W., Bitnar B., Mayor J. C., Kiess H., Lam K. H., Close J., 2007. "Efficiency model for photovoltaic modules and demonstration of its application to energy yield estimation", Solar Energy Materials & Solar Cells 91 (2007) 79–84.

IEA, 2021. *CO_2 emissions from fuel combustion highlights*. International Energy Agency, iea.org. Accessed 15 February 2021.

Incropera, F. P., Lavine A.S, Bergman T.L., Dewitt D. P., 2017. *Fundamentals of Heat and Mass Transfer*. John Wiley & Sons.

Jakhrani A. Q., Othman A. K., Rigit A. R. H., Samo S.R., Kamboh S. A., 2013. "Sensitivity Analysis of a Standalone Photovoltaic System Model Parameters". *Journal of Applied Sciences*, 13: 220-231.

King, D. L., Boyson W.E., Kratochvill J.A., 2004. *Photovoltaic Array Performance Model*, Sandia Report.

Li Z., Qiao Z., Tang T., 2018. *Numerical solution of differential equations - introduction to finite difference and finite element methods.* Cambridge University Press.

NASA, 2021. *Prediction of Worldwide Energy Resource*. National Aeronautics and Space Administration. power.larc.nasa.gov/data-access-viewer/. Acessed 15 February 2021.

Notton G., Cristofari C., Mattei M. Poggi P., 2005. Modelling of a double-glass photovoltaic module using finite differences. *Applied Thermal Engineering*, v. 25, p. 2854–2877.

Risser, V. V., Fuentes, M. K., 1984. "Linear regression analysis of flat-plate photovoltaic system performance data.", Proceedings of the 5th Photovoltaic Solar Energy Conference.

Ross, R. G., 1976. "Interface design considerations for terrestrial solar cell modules", 12th Photovoltaic Specialists Conference.

Ross, R. G., 1986. "Design techniques for flat-plate photovoltaic arrays", Proceedings of the 15th IEEE Photovoltaic Specialists Conference.

Saltelli, A., Ratto M., Andres T., Campolongo F., Cariboni J., Gatelli D., Saisana M., Tarantola S., 2008. *Global Sensitivity Analisys. The Primer*, John Wiley & Sons.

Skoplaki E., Palyvos J. A., 2009. "Operating temperature of photovoltaic modules: A survey of pertinent correlations". *Renewable Energy 34.*

Smets A. H. M., Jäger K., Isabella O., van Swaaij R., Zeman M., 2016. *Solar energy - The physics and engineering of photovoltaic conversion, technologies and systems*, UIT Cambridge.

Villalva, M. G., Gazoli, J. R., Ruppert Filho, E., 2009. "Modeling and circuit-based simulation of photovoltaic arrays", *IEEE Xplore.*

2. RESPONSIBILITY NOTICE

The authors are the only responsible for the printed material included in this paper.